High-Speed Stereo Digital Image Correlation: Application to Biaxial Fatigue

D. Busca*, M. Fazzini*, B. Lorrain*, S. Mistou*,†, M. Karama* and M. L. Pastor‡

*INP, Ecole Nationale d'Ingénieurs de Tarbes, Laboratoire Génie de Production, Université de Toulouse, 47 avenue d'Azereix, BP 1629 65016, Tarbes Cedex, France
†Parc Industriel de la Haute Bigorre, Nimitech Etudes, 1 Avenue des victimes du 11 juin 1944, 65200, Bagneres De Bigorre, France
‡UPS, IUT Tarbes, Institut Clément Ader, Université de Toulouse, 1 rue Lautréamont, BP 1624 65016, Tarbes Cedex, France

ABSTRACT: To study the behaviour of a carbon-fibre reinforced-plastic laminate under a biaxial stress state, a new type of cruciform specimen has been developed. This specimen is loaded biaxially under static and cyclic fatigue conditions. The experiments are monitored simultaneously using digital image correlation with two high-speed cameras and infrared thermography. A comparison between the measurements and a finite element model is used to validate the design of the sample.

KEY WORDS: *biaxial, composite, fatigue, infrared thermography, stereo digital image correlation*

Introduction

Composite materials are increasingly used in industry. Many experiments have developed models to allow the sizing of very complex structures. However, few experiments have characterised the behaviour of those materials under complex loading conditions, such as biaxial planar loading, and even fewer have dealt with fatigue [1]. The biaxial testing machine owned by the Laboratoire Génie de Production (LGP) laboratory allows experiments to be performed on biaxial cruciform specimens. The issue associated with such specimens is that the stress repartition is not constant over the specimen. As a result, it is challenging to obtain a full strain field measurement. Various types of monitoring techniques have already been tried and compared for such an approach [2]. Stereo digital image correlation (DIC) is a widely used technique for the measurement of a full displacement field on an extended surface during mechanical testing. For example, in [3], the technique was used to monitor the fatigue testing of cruciform specimens under biaxial loading and in [4] for the static loading of cruciform specimens. On the basis of these findings, it is believed that the stereo DIC technique seems to be an appropriate approach for monitoring such tests, because it allows the measurement of an important area of interest on a specimen with good accuracy [5]. The use of high-speed cameras also could improve the capabilities of fatigue experiments monitoring.

Furthermore, thermography is an appropriate approach for monitoring fatigue testing because it permits the measurement of increases in temperature caused by damage and hysteresis [6–8]. As developed in [9], it allows the fatigue limit of materials to be reached.

In the following study, a new kind of specimen is created in an attempt to respond better to the needs of biaxial testing and to fit with the manufacturing process. Then, this specimen is tested under static and cyclic loading conditions.

Design of the Cruciform Specimen

Material and manufacturing process

The first step of the study was to establish a process that is compatible with the kind of specimen produced. Accordingly, the Liquid resin Infusion (LRI) process seemed appropriate [10]. The primary benefit associated with this process is that it allows coupons to be produced without the use of an autoclave, which reduces the associated manufacturing cost. The principle of this process is to infuse the resin into the plies using a liquid path. The resin is taken at atmospheric pressure and then driven into the mould by the reduced pressure induced by the pump action.

The material used in this study is a carbon/epoxy composite laminate. The carbon fraction is a 12 K balanced woven fabric.

Characterisation of the material

To evaluate the suitability of the process, it was first necessary to evaluate the condition of the coupons manufactured. Initially, a rectangular plate was manufactured using the same process as that chosen to fabricate the biaxial coupons. Several kinds of coupons were sliced into this plate to determine the material characteristics.

The first type of characterisation undertaken was an evaluation of the porosity fraction, in addition to the fibre and resin mass fractions. Porosity characterisation was accomplished by performing resin dissolution [11]. The tests were run on four different samples, where two were taken in the centre of the plate (samples 1 and 2), and two were taken closer from the side of the plate (samples 3 and 4). The results are presented in Table 1. The results show that the porosity fraction was quite low (lower than 2%) and was deemed acceptable.

The samples were also characterised for the glass transition temperature (Tg). Values of Tg are measured by running differential enthalpy experiments Differential Scanning

Table 1: Resin, fibres and porosity rates and glass transition temperature measurements

Sample number			1	2	3	4
Fibres mass rate	Wf	%	69.10	72.38	77.8	70.7
Resin mass rate	Wr	%	30.89	27.61	22.16	29.30
Fibres volume rate	Vf	%	59.27	62.43	66.76	60.64
Resin volume rate	Vr	%	41.48	37.07	29.75	39.34
Porosity rate	Vo	%	−0.75	0.48	3.47	0.015
Glass transition temperature	Tg	°C	87.2	87.6	86.9	87.1

Calorimetry (DSC). The reticulation rate is primarily determined by the reticulation cycle used. The same cycle was used to manufacture all of the coupons. The tests were run on four samples, where two were taken in the centre of the plate (samples 1 and 2), and two taken closer to the side of the plate (samples 3 and 4). The results are presented in Table 1. All values were found to be adequate relative to the data specified in the technical data sheet (88 °C).

Once the material was determined to be sound, it was necessary to determine all of its mechanical constants. The parameters of interest are the Young's modulus in all directions, Poisson's ratio and the shear modulus. The mechanical constants were further used in the finite element model to design the biaxial coupon. There are several ways to determine these mechanical constants. The first which is the best known is based on uniaxial tension experiments [12]. The tests are run on five coupons in the first direction of the ply (0°), five coupons on the second direction of the ply (90°) and five coupons at 45°. Together, the set of tests allows all of the mechanical constants in the plane of the composite to be determined.

Additionally, the tests are simultaneously monitored using extensometry gauges and stereo DIC. The gauges are adhered to one side of the coupon, and the other side is used to establish a speckle pattern. In the DIC method, the trigger is applied externally using a 1-V input signal given by the tensile machine. The machine is set to send one signal for each increment of 5 kN during the experiment. At each increment, the displacements are measured and used to calculate the strains, ε, on the central area of the coupon in the two primary directions. All of the calculations were performed with the ARAMIS-V6.3.0-5 software provided by GOM [13].

In this work, the facet size measured 19 × 19 pixels, and the step size was 12 pixels in each direction. The size of the area analysed was approximately $15 \times 20\,\text{mm}^2$. The autocorrelation radius was 2.2 pixels. The mean of the strains along the tensile direction (local *x*-axis) was calculated over the area to determine Young's modulus, given the value of the load applied.

A field containing the local value of Poisson's ratio was calculated from the strain fields in both directions. The effective value of the parameter was taken as the mean of the values of this field over the surface. The value was verified to remain homogeneous over the whole surface. This method was used to calculate all of the mechanical constants. The values were then compared with those determined with the gauges and are presented in Table 2.

According to those measurements, we conclude that DIC is a reliable way to monitor mechanical experiments, such as biaxial experiments. We also notice that the standard deviation of the measurements is lower than those calculated from the gauge measurements. Additionally, it is worth noting that the moduli are slightly different in the two main directions, even though the fabric was supposed to be uniform. This peculiarity was taken into account when building the finite element model.

Finally, the out-of-plane constants were determined using ultrasonic weave measurements. The final parameter set obtained and used in the finite element model is presented in Table 3.

Finite element model

The model design was developed using the finite element software ABAQUS 6.10 [18]. Because many different designs have already been investigated [14–17], the design of the new cruciform specimen was based on those previous designs. The design criterions were as follows:

Table 2: Gauges and digital image correlation strain measurements

	Gauges				DIC			
	Young's modulus E (MPa)		Poisson's ratio ν		Young's modulus E (MPa)		Poisson's ratio ν	
Angle (°)	Mean	Standard deviation	Mean	Standard deviation	Mean	Standard deviation	Mean	Standard deviation
0	65 967	1751	0.064	0.051	65 048	755	0.059	0.018
90	69 129	812	0.047	0.054	69 904	600	0.047	0.014
45	4391	873			3625	269		

Table 3: Engineering constants of the material

E1 (MPa)	E2 (MPa)	E3 (MPa)	ν_{12}	ν_{13}	ν_{23}	G_{12} (MPa)	G_{13} (MPa)	G_{23} (MPa)
65 500	69 000	12 000	0.06	0.17	0.17	3600	4530	4530

- Stress concentration should occur only at the centre of the specimen;
- Failure should occur in the central zone due to the development of a biaxial stress state;
- The central zone must be as flat as possible for DIC measurements;
- The design must be adaptable to the LRI process;
- Ease of reproducibility; and
- Adaptability to the machine (i.e. the mechanical jaws).

To achieve this goal, a 3D finite element model was built. All of the constants determined previously were inserted into the model, taking into account the unbalanced properties of the fabric. To obtain a significant gain in the calculation time, the study was only performed on one-eighth of the model, i.e., by taking advantage of the specimen symmetries along the three main directions of the space. Two of those symmetries were due to the shape of the specimen, and the third was due to the symmetry along the thickness and the stacking sequence. A complete model also was built and was found to deliver the exact same results.

The finite element model had one element per ply in the thickness direction. The size of each element was taken as 0.5 mm in the central zone and 2 mm in the arms. As it has been demonstrated in the literature, the best way to focus the stresses into the central zone is to decrease progressively the number of plies into this area. Accordingly, the number of plies was reduced from 12 in the arm regions to four in the central zone of the coupon.

The first step was to design the shape of the coupon region held in the jaws to ensure a relatively constant stress field in the arms of the coupon. Afterward, this area was removed from the model, and the limit conditions were adapted.

Next, the model design was focused on the central region of the coupon. The elements that were modified during the design procedure were as follows:

- The thickness of the arms and the central zone;
- The width of the arms;
- The size and shape of the corners between the arms; and
- The size and shape of the central zone.

The influence of each parameter was studied independently until the model was found to fit all of the requirements. No specific optimisation method was used.

Concentrating the maximal stress at the centre of the coupon was found to be a difficult task, primarily as a result of geometrical singularities. The main criterion used to determine the acceptability of the design was the maximisation of a combined stress state, which can be calculated as the sum of the effective stresses along the primary directions. Next, it was verified that the maximum stresses along the single axes were still within the central region, where deviation to one side within that region was considered acceptable. Additionally, the stresses were verified to be constant along the thickness of the coupon, to ensure that the strains measured on the surface were consistent with the effective strains inside of the material.

Manufacturing the specimen

All of the issues associated with coupon manufacturing were developed from the need to reduce the central zone without milling the specimen after the infusion step. The reinforcement plies were cut before the moulding procedure to establish the decrease in thickness. The difficulty encountered was associated with carrying out the resin infusion step while ensuring that the central zone was held in a perfectly symmetric geometry, including the direction along the thickness. To solve this problem, we used a completely rigid mould developed in pieces. The different pieces of the mould were pressed together by administering soft vacuum around the pieces, which created the desired pressure decrease inside of the mould. The different parts of the mould were then compressed by the inward-directed force of atmospheric pressure. The resin was entered into the mould on one side and then travelled through the mould, infusing the fabric pieces, which had been previously inserted within the mould (see Figure 1). This process differs from the Resin Transfer Moulding (RTM) process by several factors: here, the resin enters the mould at atmospheric pressure and is driven through the mould by only the pressure decrease established by the pump. In an RTM process, the use of a completely rigid mould is necessary because the resin enters the mould at a higher pressure than that of the atmosphere. In this approach, the pressure drop made by the pump would be insufficient to hold the different parts of the mould together.

After the infusion step was accomplished, the mould was warmed until the correct temperature for resin reticulation. The reticulation cycle was the same as that used to manufacture the first plate, so Tg was expected to be the same.

When reticulation had been accomplished, the coupon was cut out of the plate. The porosity fraction was controlled in the remaining part of the plate and was found not to exceed 2%.

Validation of the finite element model

The specimen was then tested on the biaxial testing machine. The experiments were carried out on an Instron 8800 [19]. This equipment has four cylinders that can be controlled independently for fatigue or static loading trials. The pistons can handle a 100-kN load and have a maximum travel distance of 40 mm. This machine is driven by the WaveMatrix and Console FT applications, which allow complete static and cyclic programming of the machine. This machine has mechanical jaws.

A static tensile test was performed. The displacements were measured over the whole central region of the specimen using stereo DIC. The coupon was progressively pulled until the load of 5 kN. The force was then released, allowing the load to fall progressively back to 0 kN. The trigger was executed with the ARAMIS software, provided by GOM, which uses a macro. A photograph was collected every 0.5-kN step, yielding 10 pictures during loading and 10 pictures during unloading. Photographs were collected to ensure that the coupon was not moving inside the jaws, see Figure 1

The displacements in the central area of the specimen were measured at each step and then used to calculate the strain values by utilising the ARAMIS software [13]. The strain fields were compared with those calculated in the finite element model. The results of the DIC investigation are presented in Figure 2, whereas those obtained from finite element modelling are presented in Figure 3.

It should be noted that the fields match with a high degree of accuracy, which confirms that the model can serve as a reliable base in the following study for modelling the behaviour of the material under several loading types, such as fatigue loading.

Experimental Setup

The goal of this portion of the work was to establish a procedure that would allow biaxial fatigue experiments of the specimen, while delivering as many data points as possible to characterise the behaviour of the material. Accordingly, the experiments were monitored using simultaneous high-speed stereo DIC and infrared (IR) thermography. Stereo DIC was selected instead of DIC for all test orientations, even in-plane tests, because in a future study, this approach could be useful for detecting delamination in the specimen, which appears as an out-of-plane displacement.

High-speed stereo digital image correlation

In this study, high-speed stereo DIC was determined to be an appropriate selection for following the fatigue testing of cruciform specimens. A set of two high-speed cameras was used to collect the photographs. Both cameras were Photron Fastcam SA1.1 and were used in conjunction with the Photron Fastcam Viewer V3.0 1.08E software. The cameras are capable of 5400 frames per second at a resolution of one megapixel, which makes this approach appropriate for studying cyclic loading investigations. The imaged area of the specimen was lit by two cold spotlights. Because the shutter time was very short, it was possible to take

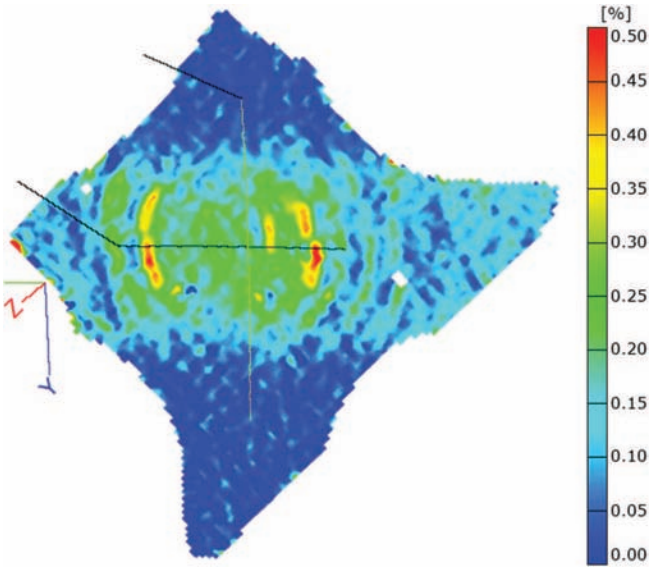

Figure 2: Strain field along the *x*-axis measured by DIC, $F = 5$kN

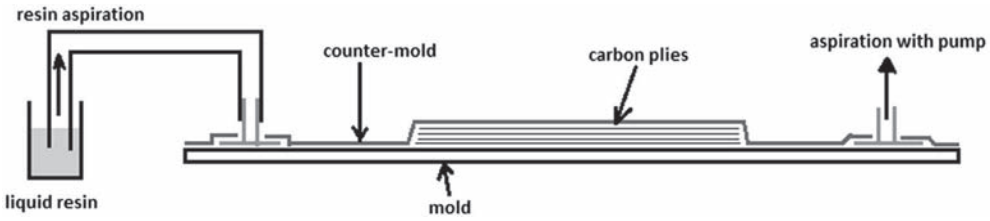

Figure 1: Description of the LRI process

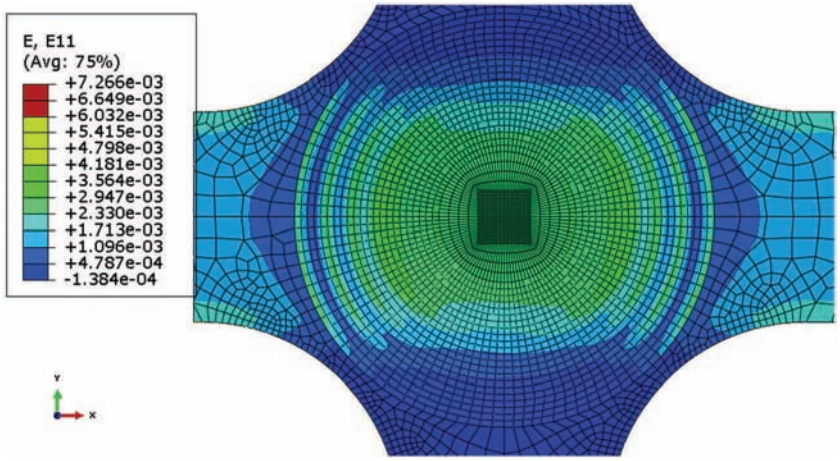

Figure 3: Strain field along the *x*-axis calculated by finite elements simulation, $F = 5\text{kN}$

consecutive pictures during the test without stopping the test. Additionally, it was possible to trigger the cameras automatically using a 10-V signal sent from the machine. Using this setup, it is possible to determine exactly when the machine sends the trigger signal, allowing the experiment to be monitored automatically. Furthermore, this approach allows pictures to be collected at different steps of the experiment: here, we applied this capability to image the specimen at the exact same time of the cycle (typically, the point at which the load was the maximum) in consecutive cycles to verify where there was any change in the strain field measured. A change would serve as a sign of the local loss of stiffness, which is typically further interpreted as a sign of local damage in the material.

The DIC was performed by the ARAMIS software [13].

In the DIC procedure, the first step was to establish adequate lighting conditions. Because the shutter time is very short (less than 1 ms) in this technique, the light on the measured area must be very intense. This was achieved by using a good position and appropriate settings for the cold spotlights. The area shot by the cameras had an approximate size of $50 \times 50\,\text{mm}^2$ with a maximal definition of 1024×1024 pixels. The stereo DIC was conducted only on the central region of the specimen, which corresponds to an area of 664×616 pixels. The frame rate of the cameras was set at 250 frames per second. The cameras were placed at a distance of 37 cm from the specimen, and the angle between the cameras was $30° \pm 1°$, as shown in Figures 4 and 5.

We used a 100-mm lens with 100-mm distance rings. To obtain the maximum amount of information during the test, 50 images were gathered per cycle. Accordingly, it was possible to obtain information for the ratio of effort/strain for several identical points at different times during the test, as well as at several points of measurement. We assumed that this number would be sufficient; it also allowed for relatively fast image treatment procedures.

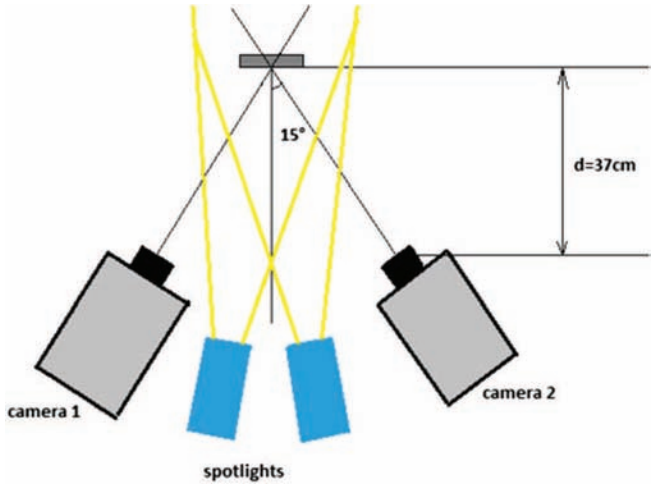

Figure 4: Stereo-DIC setup

Infrared thermography

The camera used was a Flir jade III retrofitted Titanium, with a thermic resolution of 20 mK at 30 °C. The size of the images produced is 319×254 pixels. This camera can be trigged using a 3-V signal sent by a machine, which makes it usable for automatic monitoring, as well as stereo DIC.

Additionally, because the biaxial testing machine is vertically aligned, it was possible to place the stereo DIC on one side of the specimen and the thermographic analyser on the other side. In this way, it was possible to use the analyser simultaneously when sampling the specimens, allowing the data to be coupled and compared.

All of the experiments were conducted in a temperature-controlled room. The temperature range of the room was verified not to exceed 1 °C during the test.

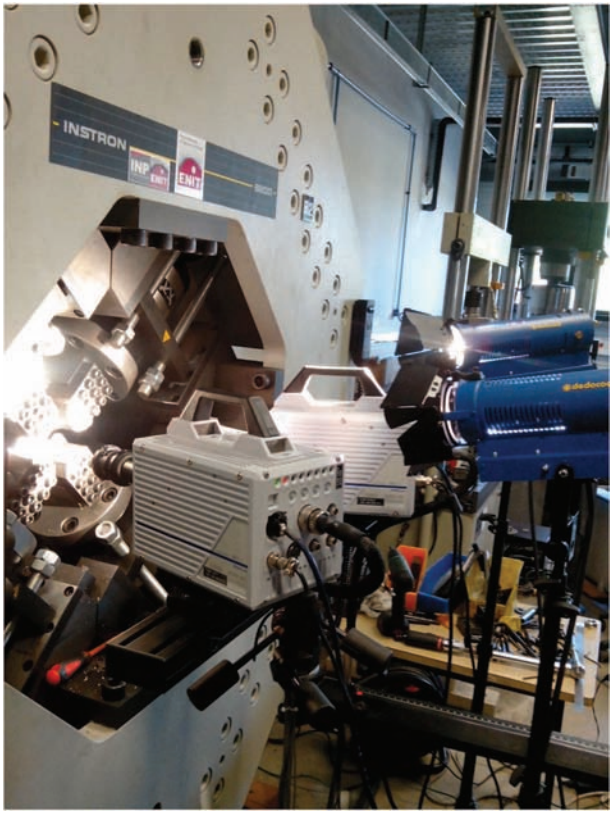

Figure 5: Picture of the stereo-DIC setup

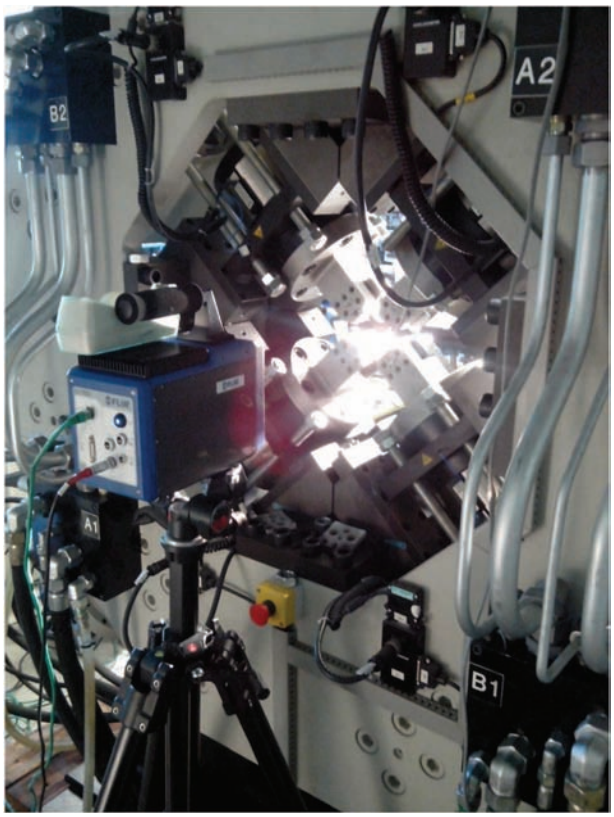

Figure 6: Picture of the IR thermography setup

The first problem encountered was interference between the warmth developed by the use of spotlights for the stereo-DIC imaging and the temperature measurements. It was necessary to determine quantitatively the amount of time after which the temperature of the coupon was stabilised to ensure that the only source of temperature elevation was the mechanical solicitation of the specimen. The tests showed that in less than 5 min, the temperature of the specimen had stabilised. The temperature increase was approximately 4 °C. However, it was necessary to repeat this procedure before each test to ensure that the temperature was stable and to prevent interference during the test, see Figure 6

Simultaneous use of stereo digital image correlation and infrared thermography

This test should not be considered a real fatigue test, because it was performed to validate the monitoring procedure that will be used for future real fatigue tests. The goal here was simply to validate that the procedure was sufficient to allow for complete and reliable monitoring of the composite fatigue tests.

The test was run on the carbon cruciform specimen presented previously. A speckle pattern was made on the central region of the specimen (Figure 7). The autocorrelation radius is 2.5 pixels. The distribution of the grey shades is shown in Figure 8.

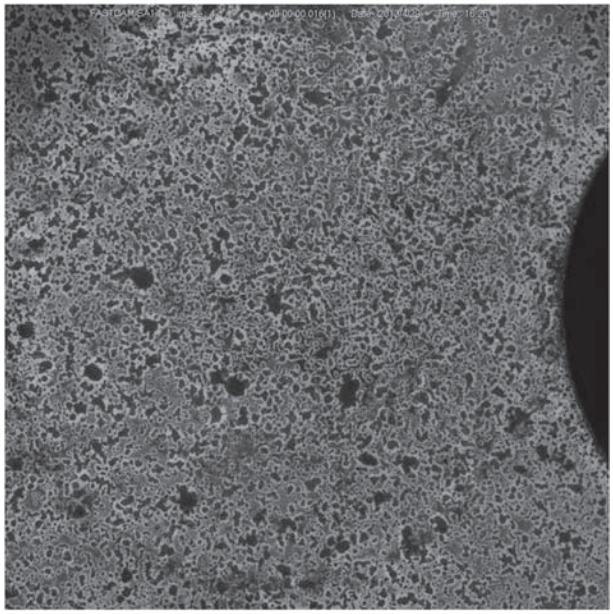

Figure 7: Picture of the speckle pattern drawn on the specimen

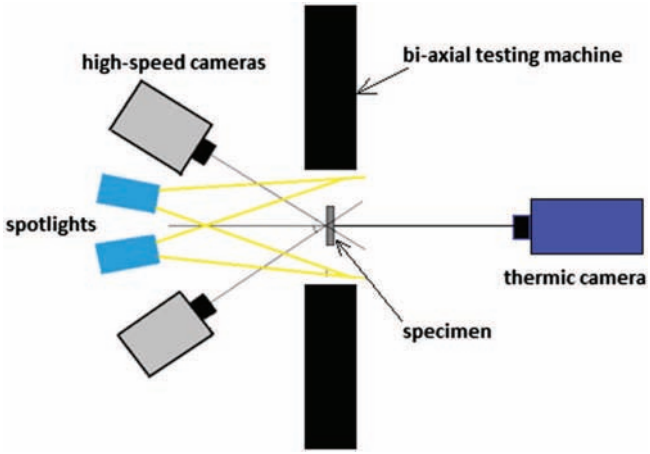

Figure 8: Experimental setup of the test

The cameras used for stereo DIC were placed on one side of the machine, and the IR camera was placed on the other side (Figure 9).

The specimen was loaded biaxially with a cyclic sinusoidal load. The average load used for the test was 5 kN with an amplitude of 3 kN. The specimens were loaded and unloaded at the same time with the same load intensity (Figure 9). According to the figure, there was a very small delay, which presents as the amplitude on the 90° axis being slightly smaller. Further improvements will be carried out to correct this delay.

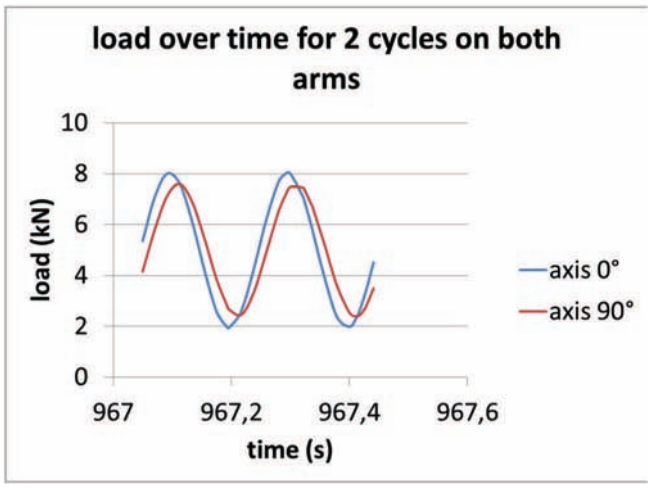

Figure 9: Evolution of the load on the main axes over time

Before the test, the temperature was stabilised even under spotlight use. A cycle was programmed into the testing machine to send a 10-V signal to the rapid cameras every 50 cycles (Figure 10). As soon as the cameras receive the signal, they collect 50 pictures at a rate of 250 fps, which means 50 images are delivered per cycle. Additionally, a picture was collected at the point of 0 kN of load at the beginning of the test. This image was used as a reference when performing the calculations.

At the same time, a 3-V signal was sent permanently to the thermic camera. With this signal, the camera takes pictures at a rate of 50 fps (10 images per cycle) but saves only one picture of each 10 pictures (one picture per cycle, Figure 10). This was used to verify that the displacement of the jaws remained stable throughout the picture sequence and can demonstrate that the pictures were collected at the exact same moment of the cycle. This parameter is important because the temperature does not remain perfectly constant over a cycle; by depending on this parameter, it was possible to ensure that the results were not skewed because of temperature variation. Additionally, we ensured that the door of the room remained closed throughout the entire test, and that the people inside the room remained in the same positions to avoid the movement of air, which could have interfered with the thermic measurements.

Results

Stereo digital image correlation

The images were treated using ARAMIS software. The goal of monitoring the fatigue loading test by using this process was to reveal the possible local loss of stiffness of the material due to damage. Accordingly, it was necessary to ensure that the images used for the calculations were taken at exactly the same point of each cycle. Taking 50 images per cycle every time allows for an accurate determination of that point, which can then be used at the same time of the cycle for each step of the test, introducing minimal error into the calculations.

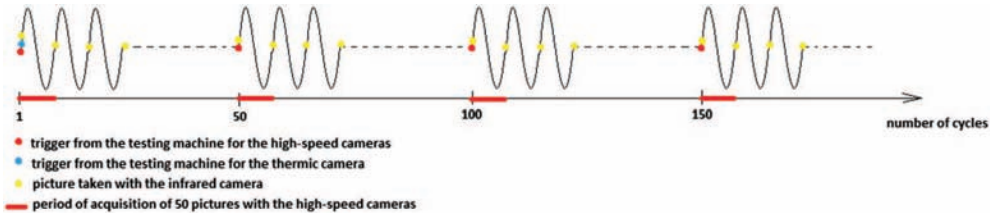

Figure 10: Algorithm of images acquisition

The facet size is 19 × 19 pixels with a step of 15 pixels in both the *X*-direction and *Y*-direction. At this step size, no deterioration of the coupon is expected. First, we validated that it was possible to collect high-quality pictures at high speed for running the stereo-DIC calculations. Next, we ensured that the calculations were run at the same point of the cycle for each step to demonstrate a real loss of stiffness.

The results of the test are presented in Figure 11 for cycle numbers 1, 100, 500, 1000, 1500, 2000, 2500, 3000, 3500, 4000, 4500 and 5000.

The curves represent the average strain along the *x*-axis for a small area in the centre of the coupon (approximately 10 × 10 pixels, Figure 12) for a complete cycle. The area was taken in the zone of interest of the coupon, where the stress state should be completely biaxial. The strains were calculated as presented in Chapter 2.2.

First, it should be noted that the curves do not start at the exact same point of the cycle because of the triggering mode. The cameras are trigged by an analogue signal, which is sent from the machine, implying that there is a small delay between the moment at which the signal is emitted and the moment at which the cameras receive the signal and then take a picture. Because of signal accuracy, this delay is not constant. Collecting 50 images per cycle allows for an accurate reconstruction of the displacement curve. The second problem is that to check the evolution of displacement during loading under different cycles, the measurement point must be manually identified on each curve to ensure that the load applied is the same. Additionally, because of the sampling frequency, this induces error because the point of measurement is not necessarily picked at the exact same loading point. By this approach, the maximal error is given by half of the amplitude of the displacement measured between two consecutive points in the area of interest. For example, the error at the peak of the sinusoid (maximum effort) is estimated to be approximately 1%.

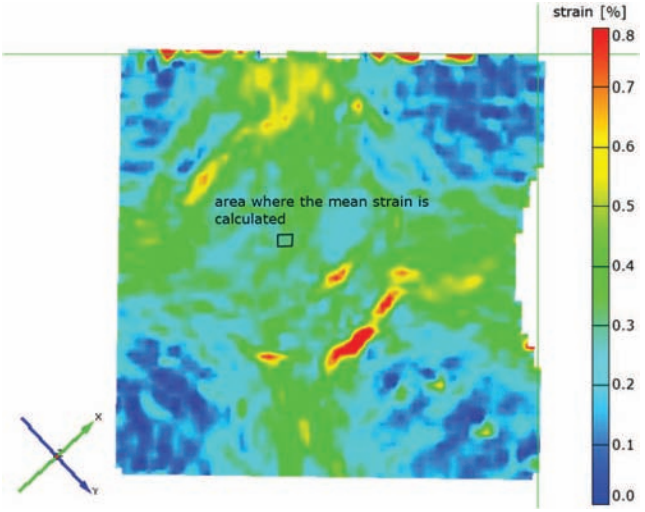

Figure 12: Repartition of the principal strains over the surface of the specimen

Figure 13 gives the minimum and maximum strains measured for each of the selected cycles as a function of the number of cycles.

On these curves, it should be noted that during the test, the strains remain constant. As mentioned earlier, this result is not surprising because of the small number of cycles used in the test. As a result, the material incurred no damage during the testing period.

Infrared thermography

Infrared thermography was used to detect damage in the structures, with the results further analysed to obtain a measurement of the thermal field of the specimen. Warming can occur as a result of two different processes, hysteresis or damage. Temperature measurements are also useful for determining the fatigue limit of a material. The goal in this work was to ensure that it would be possible to

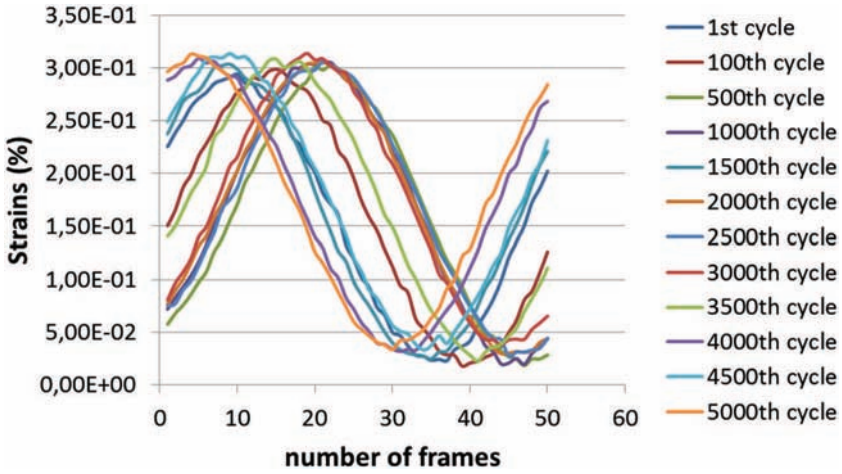

Figure 11: Evolution of the strains along the *x*-axis over a cycle for different cycles

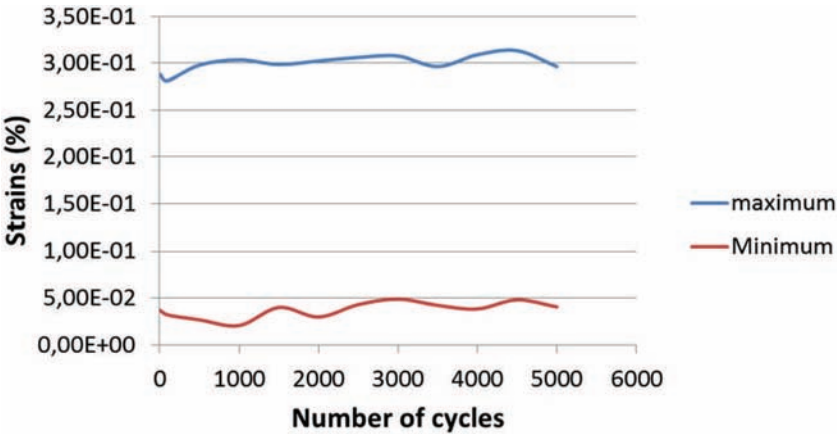

Figure 13: Evolution of the maximal and minimal strains over time

trigger the cameras at specific moments of the cycle, in addition to measuring the temperature changes on the coupon surface. The first picture is taken as the reference point. For each picture, a new field is calculated as the difference between the actual field and the reference field. It is then possible to determine visually where the temperature increases occur on the coupon.

The following curve represents the evolution of the temperature of the central surface region of the coupon. The temperature used is the average temperature of a small area and corresponds approximately to that used for the calculations presented in the DIC section (Figure 14). The curve in Figure 15 is based on all of the measurements performed, which means one measurement per cycle.

On the basis of the curve, it is possible to identify a temperature increase of approximately 0.6 °C. This increase is visible over a significant area of the coupon, although this location is where the strains were identified to be the most important in the DIC measurements. It can also be seen that the measurement suffers from noise, which might be because the movements are quite rapid; as such, a fraction of that inertia might has been dissipated as heat during the measurement. Additionally, it was difficult to discern between the different areas of interest of the coupon: the temperature increases by approximately the same amount over the whole surface. This may be because the temperature increase felt by the specimen is insufficiently low. In the future, this could be altered by increasing the

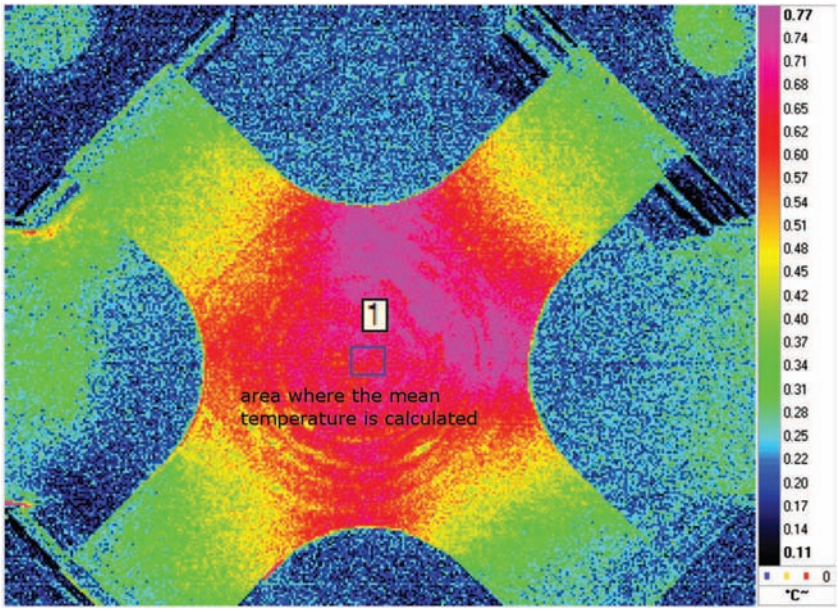

Figure 14: Repartition of the temperature increase over the surface of the specimen

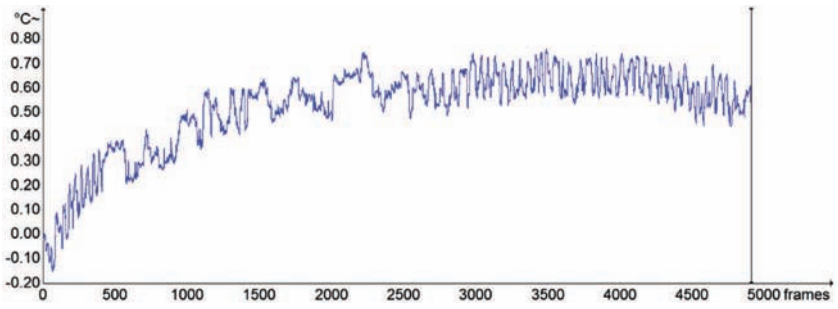

Figure 15: Evolution of the temperature over time in the central area of the specimen

maximum effort applied to the specimen during the fatigue test. It was shown in preliminary tests performed on uniaxial coupons that the increase of the temperature is highly dependent on the amplitude of the effort applied. A larger increase may deliver more prominent dispersion over the surface and may more accurately identify the critical points of the coupon.

Comparison of the measurements

Figures 12 and 14 represent for the same cycle number (i.e. 100), respectively, the scalar field of the major strain and of the temperature increase on the surface of the coupon. The recorded IR thermographic image has been transformed using a mirror along the vertical axis. This transformation was useful for performing a direct comparison of the fields, because the cameras imaged the specimen on opposite faces. In this manner, the fields are presented as if they had been imaged on the same side of the specimen, which is more useful for post-processing. Furthermore, it should be noted that the base of one of the arms (on the upper left corner of the images) was more deformed than the others. After observing the specimen further, it was noticed that a ply that should have linked the arms of the coupon was severed in the corners of this particular arm during the process. This implies that the coupon was less stiff in this particular region. This phenomenon was clearly demonstrated in both the IR thermography measurement, where the temperature was increased locally, and the DIC measurement, where the major strain was more important.

Conclusion

A new approach for monitoring fatigue experiments on composites under biaxial loading was presented. A new type of biaxial specimen was specifically designed and manufactured using an LRI process. The specimen was then tested on a biaxial testing machine under fatigue testing conditions. The test was monitored using simultaneous IR thermography and high-speed stereo DIC. This method was determined to be efficient for gathering large amounts of information with the potential to reveal the condition of the material, such as the loss of stiffness or local warming. A finite element model was established to model the behaviour of the coupon under such loading condition. This model will be used later to model the fatigue damage of the material, as well as to deliver access to the stress state of the coupon, which is not directly measurable on such a specimen. Lastly, this method will also be used later to monitor fatigue experiments on composites under uniaxial and biaxial loading conditions to identify the influence of complex loads on the behaviour of materials of interest. In a future study, variations in the IR camera triggering technique could be performed to allow for the collection of more images per cycle, as well as image collection every 50 cycles to allow the stereo DIC to obtain thermic information at each step of the loading cycle. It then might be possible to detect different thermic phenomena and to determine whether the sensitivity of the IR camera is sufficiently high for the detection of thermoelastic effects.

REFERENCES

1. Huang, Z.-M. (2002) Fatigue life prediction of a woven fabric composite subjected to bi-axial cyclic loads. *Composites part A* **33**, 253–266.
2. Ramault, C., Makris, A., Van Hemelrijck, D., Lamkanfi, E., Van Paepegem, W. (2010). Comparison of different techniques for strain monitoring of a biaxially loaded cruciform specimen. *Strain (suppl. 2)* **47**, 210–217.
3. Brault, R., Djilali, T., Fazzini, M., Mistou, S. (2010) Bi-axial fatigue analysis by stereo-correlation measurement. *EPJ Web Conf.* **6**, 16005.
4. Lamkanfi, E., Van Paepegem, W., Makris, A., Van Hemelrijck, D., Degrieck, J., Ramault, C. (2010) Strain distribution in cruciform specimens subjected to biaxial loading conditions. Part 1: two-dimensional versus 3-dimentional finite element model. *Polym. Test.* **29**, 7–13.
5. Bornert, M., Brémand, F., Doumalin, P., *et al*. (2008) Assessment of digital image correlation measurement errors: methodology and results. *Exp. Mech.*. DOI: 10.1007/s11340-008-9204-7.
6. La Rosa, G., Risitano, A. (2000) Thermographic methodology for rapid determination of the fatigue limit of materials and mechanical components *Int. J. Fatigue* **22**, 65–73

7. Toubal, L., Karama, M., Lorrain, B. (2006) Damage evolution and infrared thermography in woven composite laminates under fatigue loading. *Int. J. Fatigue* **28**, 1867–1872.
8. Steinberger, R., Valadas Leitao, T. I., Ladstätter, E., Pinter, G., Bilinger, W., Lang, R. (2006) Infrared thermography techniques for non- destructive damage characterisation of carbon-fiber reinforced polymers during tensile fatigue testing *Int. J. Fatigue* **28**, 1340–1347.
9. Toubal, L. (2004) Approaches analytique et expérimentale de l'endommagement par fatigue d'un composite carbone/epoxy *thèse de l'Université Toulouse 3*, *Paul Sabatier*.
10. Berbain, F., Chevalier, A. Mise en œuvre des composites, *Techniques de l'ingenieur, traité Plastiques et Composites, A 3 720*.
11. EN2564-Détermination de la teneur en fibres et du taux de porosité
12. NF EN ISO 527 determination des propriétés en traction
13. Aramis software (2006) GOM Optical measuring techniques, http://www.gom.com.
14. Escárpita, A., Elizalde, H., Ramirez, R., Ledezma, E., Pinho, S. (2010) Modified cruciform specimen for bi-axial testing of fibre reinforced composites. *40° congreso de investigacion y desarrollo Mexico*, 232–232.
15. Smits, A., Van Hemelrijck, D., Philippidis, T. P., Cardon, A. (2006) Design of a cruciform specimen for biaxial testing of fiber reinforced composite laminates. *Compos. Sci. Technol.* **66**, 964–975.
16. Van Hemelrijck, D., Smith, A. (2003) Biaxial testing of fiber-reinforced composites, *16TH international conference on composite materials*.
17. Welsh, J. S., Adams, D. (2002) An experimental investigation of the bi-axial strength of IM6/3501-6 carbon/epoxy cross-ply laminates using cruciform specimens. *Composites Part A* **33**, 829–839.
18. Abaqus software. Dassault systems Simulia. http://www.3ds.com/fr/produits-et-services/simulia/portefeuille/abaqus/
19. Instron. http://www.instron.tm.fr